DOI:10.1190/segam2021-3588114.1

# Learnings from an FWI Imaging study using 3D and 4D data over a post-salt field in Campos Basin

*Samanta Bortoni*, Sergio Barragan, Gregório Azevedo, Luis Cypriano (CGG); André Ferreira, Wendel Moreira, Paula dos Reis, Wilson Filho (PETROBRAS)*

**Summary**

Seismic images obtained through conventional migration methods have limitations such as amplitude distortions and migration artifacts. To mitigate these limitations, we can generate full-waveform inversion (FWI) images by computing the reflector-normal derivatives of the high-frequency FWI velocities. Given the resolution, accuracy, and geological consistency of the velocities obtained from Time-lag FWI (TLFWI), FWI Images can be comparable to traditional migration images. Thus, we present the advantages of 3D FWI Images over conventional RTM images when dealing with geological obstructions. By computing FWI Images from the individual FWI velocity models of both baseline and monitor surveys, we can also illustrate the benefits of FWI Imaging for 4D by retrieving more continuous amplitudes at the reservoir level and analyze the effects of using respective baseline and monitor velocities in 4D images.

**Introduction**

Thirty-five years ago, Tarantola (1986) suggested that the future of seismic data would rely on direct inversion of material properties of the Earth as opposed to simple migrations. Although velocity inversions have become widespread, seismic images are still obtained by methods such as Kirchhoff or reverse-time migration (RTM), in which data is considered to only consist of first-order events (i.e., primaries). Compared to inversion algorithms, the adjoint operators from both Kirchhoff and RTM yield images that are more susceptible to poor illumination and migration artifacts. Least-squares migration (LSM) reframes these adjoint-only methods as inversions, which generally improves the image. However, LSM still relies on the (linear) first-order Born approximation to the full wave propagation, which only accounts for primaries, not multiples or diving waves.

Full-waveform inversion (FWI), on the other hand, is an iterative inversion of the full wavefield, often applied in a multi-scale sense (with increasing frequency, and thus wavelength). Since it relies on the full wavefield, FWI includes not only primaries but refractions, multiples, and guided waves, among others. These features make it an attractive tool for illuminating the subsurface in the presence of surface acquisition obstructions or geological shadow-zones that are poorly illuminated by primary energy. It has been shown that FWI can derive small-scale variations in velocity (e.g., Virieux and Operto, 2009; Wang et al., 2019), filling the historical resolution gap (Claerbout, 1985) between inversion of velocities and reflectivities.

Traditionally, FWI-derived velocity models are largely used for their kinematic properties as input for migration. However, rapid expansion in computational resources has allowed us to obtain inversions at high frequencies, from which a reflectivity representation of the subsurface may be estimated. These so-called FWI Images are obtained by computing the reflector-normal gradient of the velocity (Zhang et al., 2020).

Mature reservoirs benefit from periodic monitoring to assess production, optimize well placement, manage injections, and maximize recovery. Time-lapse (4D) seismic is a cost-effective technology that can provide insight into these processes. Accurate 4D images can help estimate fluid changes, thus improving reservoir management. 4D signal is traditionally measured from conventionally migrated images of baseline and monitor surveys, often using the same velocity model in both migrations. In contrast, we generate the 4D FWI Image directly from the monitor and baseline FWI Images by computing their difference.

In this work, we illustrate some advantages of FWI Imaging over conventional RTM using a streamer data set from offshore Brazil. Additionally, we validate the accuracy of the FWI velocity when compared to sonic logs, demonstrate improvements in 3D illumination and 4D amplitudes, and analyze the effects of velocity changes on 4D.

**Methodology**

We applied FWI Imaging in a deep-water Campos Basin post-salt reservoir using narrow-azimuth towed-streamer (NATS) data from 2005 and 2018. Both surveys kept the same azimuthal coverage and nominal fold, being limited to a 6 km streamer length. We employed Time-lag FWI (TLFWI), which is robust against cycle-skipping and noise and is not overly sensitive to amplitude inconsistencies (Zhang et al., 2018; Wang et al., 2019). With the smoothed legacy velocity (based on tomographic inversions) as an initial model, we inverted separate velocity models for each survey. At 10 Hz, following the method in Hicks et al. (2016), we created a common model by averaging the velocity models of both surveys. With this, we intend to direct both inversions to similar local minima and improve the 4D response. For the 4D analysis, baseline and monitor

were inverted up to 20 Hz, and for the 3D we further inverted the baseline up to 30 Hz.

We approximate the reflectivity by computing the reflector-normal derivative of the velocities (Zhang et al., 2020). Baseline and monitor FWI Images, as well as FWI 4D differences, were generated according to the simplified flow described in Figure 1. Given the resolution, accuracy, and geological consistency of the velocities obtained from TLFWI (Figure 2), we consider that the outcome of the velocity derivative is comparable to traditional migration images.

**Results and discussions**

To demonstrate the accuracy of the inversions, the 30 Hz baseline TLFWI velocity model is compared with a legacy velocity model and a sonic log profile available in the area (Figure 2).

While the legacy velocity model is quite smooth (Figure 2a), characterized by the low-wavelength updates from tomography, the FWI velocity model (Figure 2b) presents a detailed representation of the structures. From a smoothed version of the legacy velocity model, we invert with TLFWI up to 30 Hz. The result shows strong correlation with the sonic log in the area (Figure 2c). It is important to note, however, that this behavior is most likely to happen when elastic effects are negligible and in areas where the geology does not deviate strongly from Gardner's relation between densities and velocities. It is plausible that these conditions are better satisfied in the post-salt level than in salt or pre-salt levels.

By differentiating the baseline velocity, we generated a 30 Hz FWI Image, which we then compared with the corresponding RTM image. The 3D FWI Image has a more balanced amplitude distribution, showing improvements in illumination. Figure 3 displays an example of a geological obstruction, possibly an injected sandstone (yellow circles). As a diffracting body, injectites can deteriorate amplitudes provided by conventional migration methods, which consider linearized Born scattering. In Figure 3a, the 30 Hz RTM image presents a cone of poor illumination below the geological obstruction. This affects the amplitudes of the image at the reservoir level, denoted by the yellow arrow. When looking at the FWI Image (Figure 3b), we see that the amplitudes are more continuous and better balanced below the injectite. Furthermore, FWI Imaging presents higher S/N and cleaner events. Depth slices in Figures 3c and 3d show how the amplitudes are more balanced compared with the RTM image.

Figure 4 illustrates the 4D amplitudes for the same section. The strong amplitude reflector below the injectite is possibly an indicator of fluid changes, which are not expected to occur in the injectite itself. At the right of this reflector is another possible true 4D signal, while elsewhere we most likely have 4D noise. The 4D images were derived without any adjustments or matching between baseline and monitor.

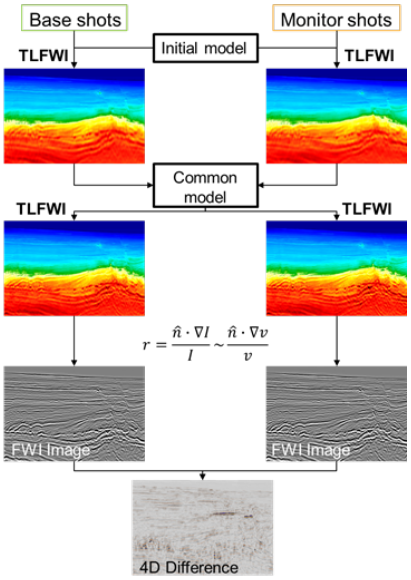


Figure 1: FWI Image workflow

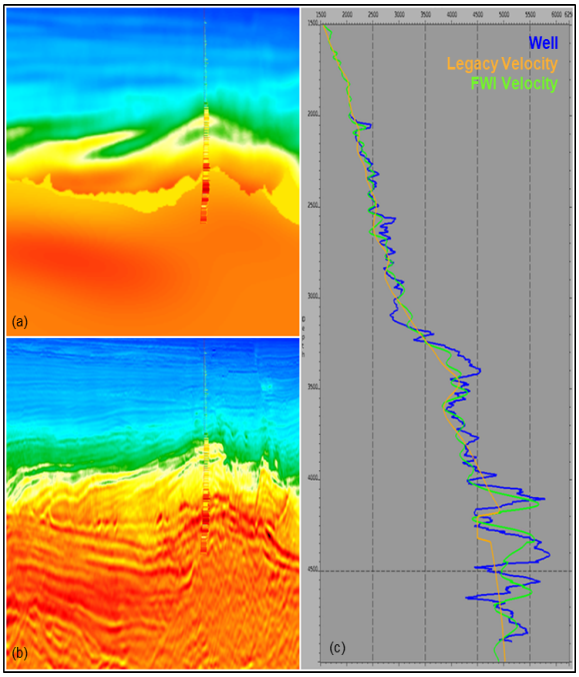


Figure 2 (a) Legacy velocity; (b) FWI velocity; (c) Comparison between legacy velocity, FWI velocity, and well sonic.

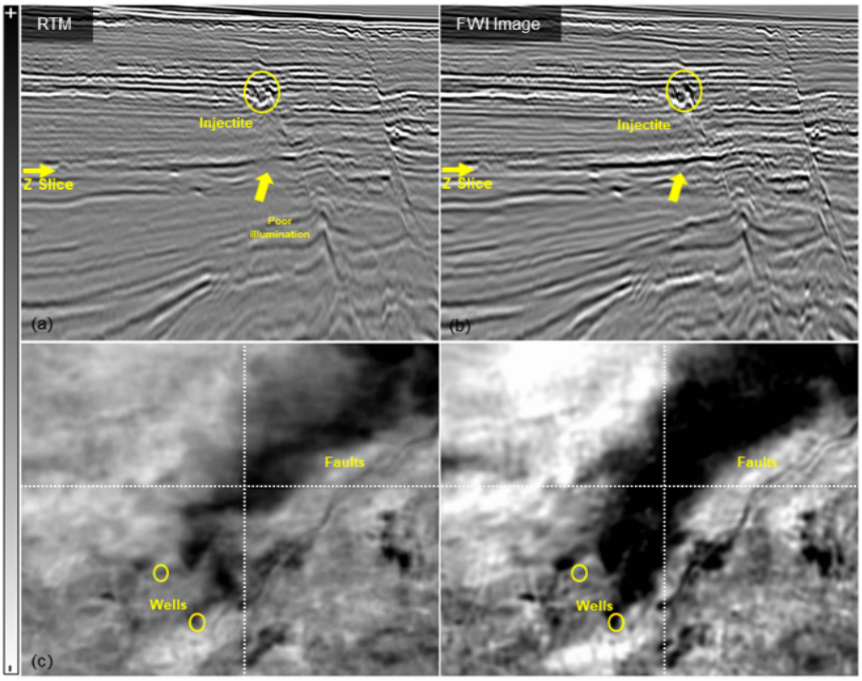


Figure 3: Illumination below geological obstruction (a) 30 Hz baseline RTM stack inline view; (b) 30 Hz baseline FWI Image inline view; (c) 30 Hz baseline RTM stack depth-slice view; (d) 30 Hz baseline FWI Image depth-slice view.

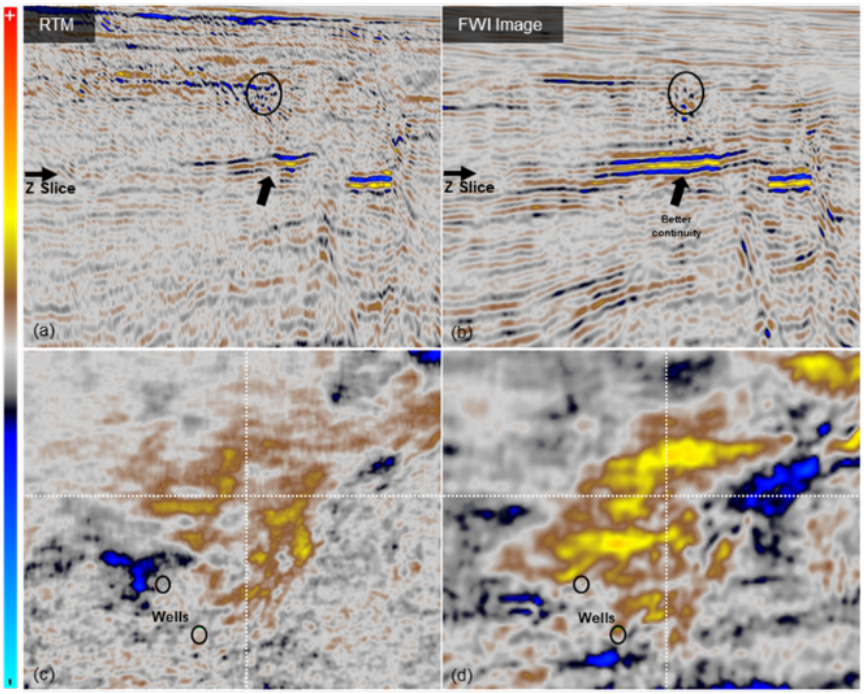


Figure 4: 4D signal amplitudes (a) 4D 20 Hz RTM stack inline view; (b) 4D 20 Hz FWI Image inline view; (c) 4D 20 Hz RTM stack depth-slice view; (d) 4D 20 Hz FWI Image depth-slice view.

Figure 4a shows the 4D RTM, in which amplitudes are weak and discontinuous at the reservoir level. In Figure 4b, the 4D FWI Image has more continuous amplitudes and weaker noise in the overburden (also perceived in the NRMS maps of Figure 6), which may potentially improve the interpretation. However, residuals are relatively strong in the deeper section near salt bodies. The depth slices show that strong positive amplitudes related to 4D signal have more extension in the FWI Image, getting closer to the wells and extending further beyond the dashed inline.

As the 4D FWI Image is the difference between velocity derivatives from the baseline and monitor, it accounts for velocity changes in the reservoir, thus avoiding 4D noise caused by erroneous propagation at and below the reservoir. Figure 5 displays another 4D section, where we exemplify this problem. In Figure 5a, reservoir velocity changes between the baseline and monitor were not considered. As a result, we observe a vertical error propagating below the reservoir in the 4D RTM image. In Figure 5b, the FWI Image has a cleaner 4D image below the reservoir as the 4D time-shifts are naturally corrected by the TLFWI velocity models. However, stronger residuals can be observed in the deeper section in the presence of salt reflectors.

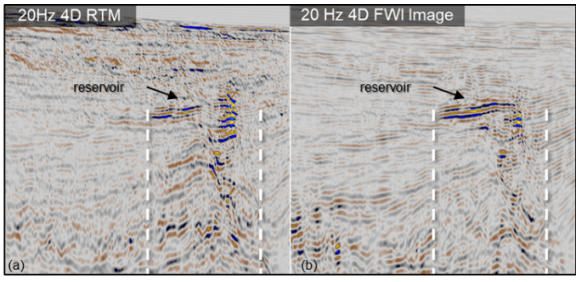


Figure 5: Effect of 4D velocity changes: (a) 4D 20 Hz RTM stack; (b) 4D 20 Hz FWI Image. Dashed vertical lines indicate the region of 4D timeshift below the reservoir in the RTM image.

As a general quality control, we extracted the NRMS above the reservoir level as a measurement of repeatability. Figure 6a shows the NRMS map and histogram for the 4D RTM image; Figure 6b shows the same for the 4D FWI Image. The NRMS maps show better repeatability between the FWI Image vintages, denoted by the median value decreasing when compared to the 4D RTM (from 15.7% to 14.2%).

To quantify the impact of reservoir velocity changes captured in the TLFWI velocity models, we extracted the time-shifts at deeper levels. As observed, the time-shifts for the FWI Image (Figure 6d) are lower than for the RTM (Figure 6c). Results show a reduction in both median values, from 0.4 ms to 0.2 ms, and standard deviations, from 1.8 ms to 0.9 ms. A strong decrease is observed for the positive time-shifts in the center of the map (highlighted by the grey arrow), which is located below the expected 4D signal.

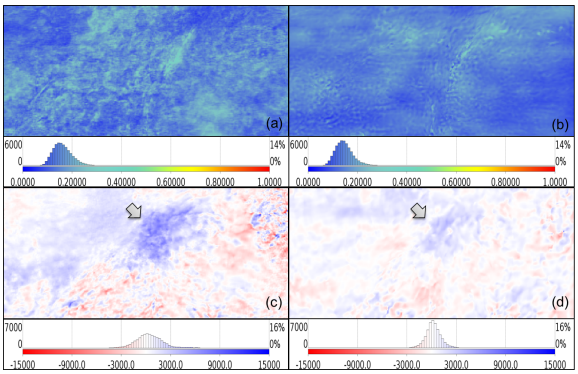


Figure 6: 4D QC maps: NRMS above the reservoir from (a) RTM and (b) FWI Image; Time-shifts below the reservoir from (c) RTM and (d) FWI Image.

## Conclusions

FWI Imaging is a full-wavefield, multi-scale, non-linear inversion that may be suitable for areas suffering from incomplete or variable 3D illumination. With reduced sensitivity to illumination problems, it benefits 4D seismic monitoring, where illumination is often non-repeatable. It may also improve 4D images given the higher S/N and amplitude balancing when compared to standard migrations.

We have demonstrated these benefits using 4D NATS data; however, it is important to validate these observations with other types of acquisitions. Additionally, this study focused on post-salt reservoirs, so pre-salt reservoirs and other areas with more complex geology need to be considered for further studies. Special attention to salt boundaries, where we observed strong residuals in our results, is needed in further work. Elastic effects were not taken into consideration as we used the acoustic wave equation for wave propagation. This can bias the amplitudes of the FWI Image in places where density and/or shear velocity contrasts are influential (e.g., at salt boundaries). As such, amplitude fidelity needs to be carefully examined.

The 4D results for the FWI Image in this study were limited to 20 Hz. Increasing the frequency limit is still challenging since higher frequencies are more sensitive to kinematic errors between the baseline and monitor velocity models. Finally, FWI Imaging is computationally more intensive than RTM or LSRTM. This may limit the frequencies achievable in practice, especially for larger surveys.

## Acknowledgments

We thank CGG and Petrobras for permission to publish this work.

## References


Claerbout, J. F., 1985, Imaging the Earth's Interior: Blackwell Scientific Publications.

Hicks, E., H. Hoeber, M. Houbiers, S. P. Lescoffit, and A. Ratcliffe, 2016, Time-lapse full-waveform inversion as a reservoir-monitoring tool — A North Sea case study: The Leading Edge, **35**, 850–858, doi: https://doi.org/10.1190/tle35100850.1.

Tarantola, A., 1986, A strategy for nonlinear elastic inversion of seismic reflection data: Geophysics, **51**, no. 10, 1893–1903, doi: https://doi.org/10.1190/1.1442046.

Virieux, J., and S. Operto, 2009, An overview of full-waveform inversion in exploration geophysics: Geophysics, **74**, no. 6, WCC1–WCC26, doi: https://doi.org/10.1190/1.3238367.

Wang, P., Z. Zhang, J. Mei, F. Lin, and R. Huang, 2019, Full-waveform inversion for salt: A coming of age: The Leading Edge, **38**, 204–213, doi: https://doi.org/10.1190/tle38030204.1.

Zhang, Z., J. Mei, F. Lin, R. Huang, and P. Wang, 2018, Correcting for salt misinterpretation with full-waveform inversion: 88th Annual International Meeting, SEG, Expanded Abstracts, 1143–1147, doi: https://doi.org/10.1190/segam2018-2997711.1.

Zhang, Z., Z. Wu, Z. Wei, J. Mei, and R. Huang, 2020, FWI Imaging: Full-wavefield imaging through full-waveform inversion: 90th Annual International Meeting, SEG, Expanded Abstracts, 656–660, doi: https://doi.org/10.1190/segam2020- 3427858.1.